Langmuir

ARTICLE

pubs.acs.org/Langmuir

Membranes of Vertically Aligned Superlong Carbon Nanotubes

Feng Du,[†,‡] Liangti Qu,[‡,§] Zhenhai Xia,[∥] Lianfang Feng,[⊥] and Liming Dai[*,†,‡]

[†]Department of Macromolecular Science and Engineering and Department of Chemical Engineering, Case School of Engineering, Case Western Reserve University, 10900 Euclid Avenue, Cleveland, Ohio 44106, United States

[‡]Department of Chemical and Materials Engineering, School of Engineering, University of Dayton, 300 College Park, Dayton, Ohio 45469, United States

[§]Key Laboratory of Cluster Science, Department of Chemistry, School of Science, Beijing Institute of Technology, Beijing 100081, People's Republic of China

[∥]Department of Materials Science and Engineering, University of North Texas, Denton, Texas 76203, United States

[⊥]State Key Laboratory of Chemical Engineering, Department of Chemical and Biological Engineering, Zhejiang University, Hangzhou 310027, China

ABSTRACT: In the present work, we have developed a simple but effective method to prepare superlong vertically aligned carbon nanotubes (SLVA-CNT) and epoxy composite membranes, and we have demonstrated that various liquids, including water, hexane, and dodecane, can effectively pass through the SLVA-CNT membranes. These results were confirmed by molecular dynamics simulations. While the mechanical densification was used to further enhance the flow transport through the SLVA-CNT membranes, we developed in this study a magnetic-nanoparticle switching system to turn on and off the flow through the nanotube membrane by simply applying an alternating voltage. The methodologies developed in this study should have a significant implication to the development of various smart membranes for advanced intelligent systems.

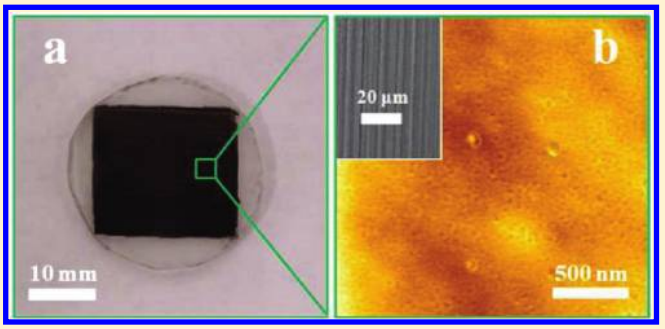

INTRODUCTION

Carbon nanotubes (CNTs) are a class of attractive nanomaterials, including single-walled carbon nanotubes (SWNTs) and multiwalled carbon nanotubes (MWNTs). While a SWNT may be conceptually viewed as a graphene sheet that is rolled into a nanoscale tube form, a MWNT consists of additional graphene coaxial tubes around the SWNT core.[1] Depending on their diameter and the chirality of the orientation of graphene rings along the nanotube length, carbon nanotubes may exhibit semiconducting or metallic behavior to allow them to be used for many potential applications, including as conductive materials, electromagnetic and microwave absorbing coatings, high-strength composites and fibers, sensors, field emission displays, energy storage and energy conversion devices, radiation sources and nanometer-sized semiconductor devices, interconnects, and multifunctional membranes.[2−6] For most of the above-mentioned and many other applications, it is highly desirable to prepare aligned/micropatterned CNTs. Particularly, vertically aligned carbon nanotubes (VA-CNTs) can provide a well-defined large surface area and be readily incorporated into various device configurations. For instance, well-ordered nanoporous membranes can be prepared by simply filling the gaps of the VA-CNT "forest" with polymers, followed by opening the nanotube ends. By incorporating a high-density array of VA-MWNTs across a solid polystyrene film and opening the nanotube end caps at both sides (e.g., by plasma etching), Hinds and co-workers[7] have successfully prepared VA-MWNT membranes. These authors further demonstrated that pressure-driven liquid flow can pass through the VA-MWNT membrane with a flow rate that is 4−5 orders of magnitude faster than a simple macroscopic membrane. Several other groups have also investigated various nanoscale membranes, including those based on CNTs.[8−11] On the other hand, rapid mass transport across carbon nanotubes has also been predicted by theoretical studies.[12] The enhanced mass transport has been attributed to confinement-induced liquid phase transitions and/or atomic smoothness of the CNT wall, which leads to more specular reflection to allow the flow molecules to retain their original momentum after collision with the nanotube wall. Carbon nanotube-based membranes are intriguing since their pore size can be precisely controlled by controlling the size of catalytic particles used for nanotube growth, and the polarity of the pore can be tuned through region-selective functionalization, as demonstrated by Hinds[13] and others.[14−16]

The recent availability of superlong vertically aligned carbpn nanotubes (SLVA-CNTs) with millimeter-order nanotube lengths could offer significant advantages over their shorter counterparts

Received: March 16, 2011
Revised: May 25, 2011
Published: June 09, 2011

for various potential applications,[17−21] including their use for flow transport, water−oil separation, nanoparticle separation, and voltage generation. The millimeter-order nanotube lengths should simplified the design and development of novel CNT-based membranes by fully coating the SLVA-CNTs with a polymer matrix, followed by cutting off the polymer-wrapped CNTs at both ends. In addition, the long nanotube length could facilitate the asymmetric end functionalization[15,22] and mechanical densification[23] of the SLVA-CNT arrays. Furthermore, their millimeter-order lengths provide new opportunities for transporting liquids/gases and flow-induced voltage generation[18] through individual nanotubes over large length scales. Therefore, it is important to develop membranes based on the SLVA-CNT arrays for many existing and novel applications. As far as we are aware, however, there is no discussion on either membrane development or mass transport through SLVA-CNT membranes in the literature.

We have recently found that various liquids, including water, hexane, and dodecane, can effectively pass through the SLVA-CNT membranes. These results were confirmed by molecular dynamics simulations. While the mechanical densification[23] was also used to further enhance the flow transport through the SLVA-CNT membranes, a magnetic-nanoparticle switching system developed in this study enabled us to turn on and off the flow through the nanotube membrane by simply applying an alternating voltage. In this paper, we report the detailed preparation and characterization of the first membrane based on SLVA-CNTs, along with experimental and theoretical studies on flow characteristics through the SLVA-CNT membrane.

EXPERIMENTAL SECTION

Materials and Characterization. Iron nanoparticles were purchased from Sunano Company; they are well dispersed in water by a probe processor with 0.1% Triton X-100 (Acros reagent). $HAuCl_4 \cdot 3H_2O$ from Alfa Aesar and deionized ultrafiltered water from Fisher Scientific Co. were used for the preparation of gold nanoparticles. Gold nanoparticles of 13 nm were synthesized by reducing $HAuCl_4 \cdot 3H_2O$ with sodium citrate in an aqueous solution according to published procedures.[24]

Scanning electron microscope (SEM) images were recorded on a Hitachi S-4800 high-resolution SEM unit, while transmission electron microscope (TEM) imaging was performed on a Hitachi H-7600 TEM. Atomic force microscopy (AFM) measurements were taken on a Pacific Nanotechnology Micro 40.

SLVA-CNT Synthesis. The several millimeter long vertically aligned SLVA-CNTs were synthesized onto a SiO_2/Si wafer from Fe catalyst by the water-assisted chemical vapor deposition (CVD) technique[17,19,20] with high-purity (99.99%) ethylene as the carbon source and He/H_2 (2.5:1 v/v) as a carrier gas under 1 atm pressure at 760 °C for about 10 h. A thin (10 nm) Al_2O_3 buffer film was used between the SiO_2/Si substrate and the Fe catalyst layer (1 nm thick).[19,20] During the nanotube growth process, a controlled amount of water vapor was also introduced into the carrier gas at concentrations in the range of 200−400 ppm. The SLVA-CNT arrays were produced under optimized conditions, as described elsewhere.[19,20]

Preparation of SLVA-CNT Membranes. In a typical experiment, the as-synthesized SLVA-CNT (7 mm long) film on a SiO_2/Si substrate was placed in a polystyrene Petri dish containing epoxy resin (Epon 828 and Jeffamine D 230, 3:1 by weight). The solvent-free, low-viscosity epoxy mixture penetrated into the CNT matrix and filled up the vacancy in the matrix under vacuum (∼100 Torr). The epoxy mixture was then degassed to remove air bubbles. Thereafter, excess polymer was removed until the nanotube array was exposed, followed by curing at room temperature for 24 h. Then, the nanotube ends in the membrane were opened by simply hand-cutting with a knife (Figure 1a). The resultant nanotube array impregnated with the cured epoxy coating was taken out of the Petri dish, and the Si substrate was peeled off. The newly exposed surface was treated with HF to open the nanotube ends by removing the residual catalyst, if any. The resultant CNT/epoxy composite membrane is shiny, flat, and crack-free. To investigate the CNT packing density effect, we first remove the SLVA-CNT array from the Si substrate by etching the nanotube/Si interface with HF vapor. Subsequent mechanical compression of the free-standing SLVA-CNT array uniaxially led to an increase in the nanotube packing density.[23] The compressed SLVA-CNT array was then used to prepare the CNT/epoxy composite membrane according to the procedure described in Figure 1b.

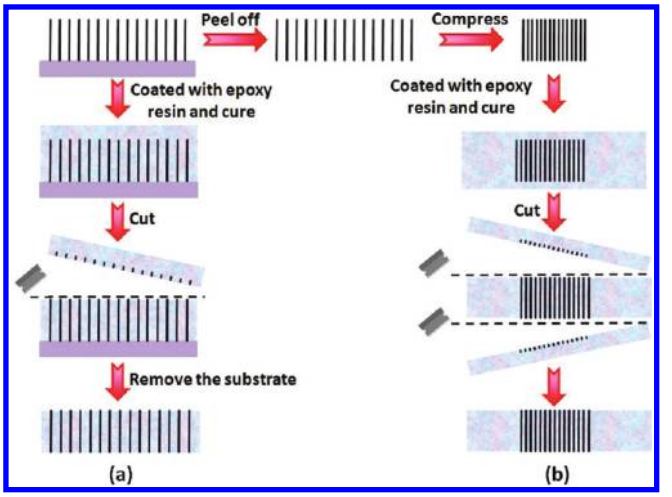

Figure 1. Schematic representation of preparation procedures for the as-synthesized membrane: (a) before and (b) after mechanical compression.

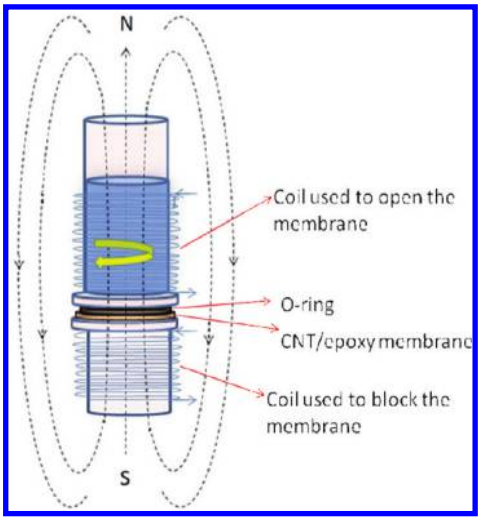

Figure 2. Schematic representation of the solenoid used to switch the membrane on/off magnetically.

Leakage Testing. Prior to the measurements of flow characteristics through the CNTs in SLVA-CNT/epoxy composite membranes, we carefully tested for any possible leakage within the polymer matrix by filtering solutions of nanoparticles with various sizes (e.g., 13 nm gold nanoparticles, 25 nm iron nanoparticles) larger than the nanotube diameter through the membrane. The permeated solution was then compared with the feed solution by UV−vis measurements to ensure there is no leakage in the polymer matrix. In addition, dye molecules

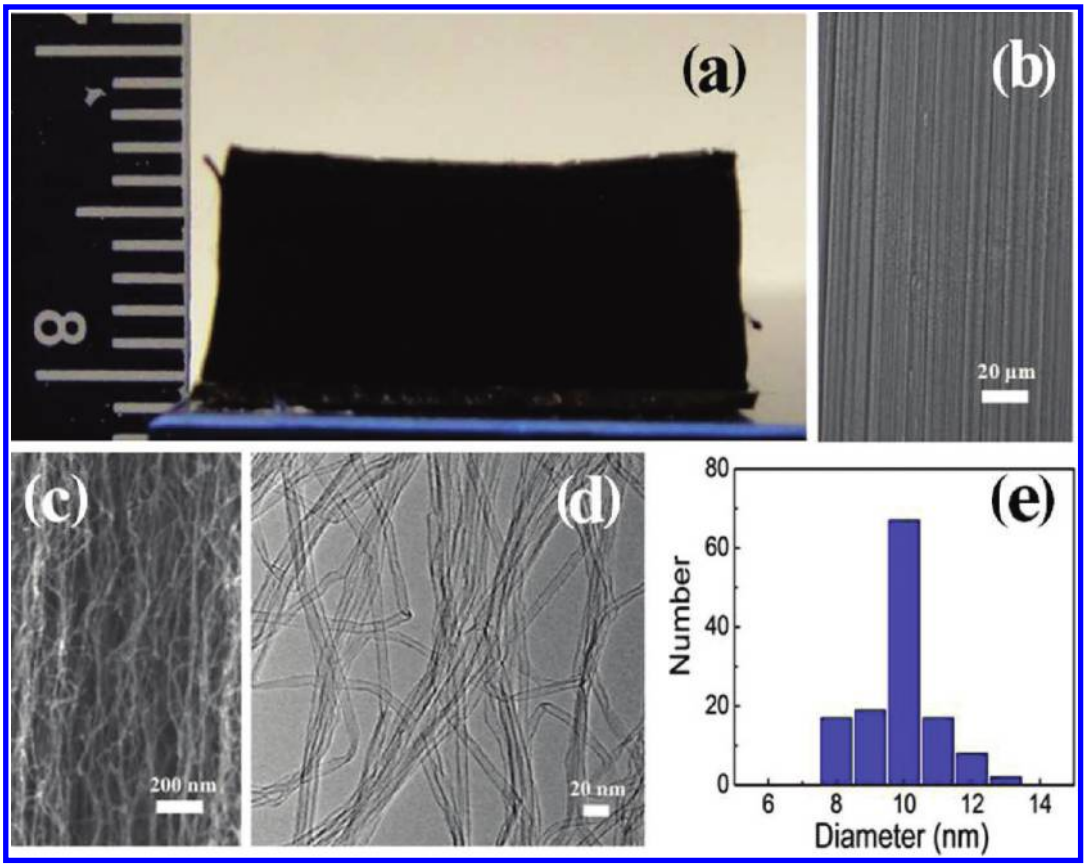

Figure 3. SLVA-CNTs used in this study: (a) digital photograph of the 7 mm long SLVA-DWNT array; (b, c) cross-sectional SEM images of the SLVA-CNTs under different magnifications; (d) TEM image of the superlong CNTs after having been dispersed in ethanol and deposited on a copper TEM grid without carbon film, showing an inner diameter around 10 nm; and (e) histogram showing the diameter distribution measured from TEM images for the SLVA-CNTs .

(i.e., 2-naphthalenesulfonic acid hydrate) were mixed into the epoxy matrix during the membrane preparation to confirm a noncrack structure in the epoxy matrix and the flow passing through nanotube inner core only, which otherwise will release dye molecules trapped in the polymer matrix.

Electric/Magnetic Field-Induced Switching. In order to demonstrate the switching capability for SLVA-CNT/epoxy composite membranes, we designed and developed a solenoid using RadioShack 30-gauge enamel-coated magnet wires wrapped around a filter holder to produce a magnetic field by applying an electric current. As can be seen in Figure 2, the solenoid with a diameter around 4 cm consists of coils with 1200 turns/2.3 cm (520 turns/cm) and 834 turns/1.8 cm (462 turns/cm) above and below the membrane, respectively. O-ring and clamp were used to seal the membrane in the filter holder. By mixing the 25-nm iron nanoparticles in the flow inside the filter holder above the membrane (Figure 2), the magnetic iron nanoparticles with a size larger than the nanotube inner diameter (~10 nm, see below) will act as a stopper to open/block the CNT membrane by moving up/down along the magnetic field when an alternating voltage is applied.

Effects of CNT Packing Density. As schematically shown in Figure 1b, mechanical compression[23] was used to increase the CNT packing density for investigating possible packing density effects on the flow behavior through SLVA-CNT/epoxy composite membrane.

RESULTS AND DISCUSSION

Figure 3a shows a typical optical microscopic image for a 7 mm long SLVA-CNT array. The corresponding SEM images under different magnifications given in Figure 3b,c clearly show the well-aligned individual nanotubes closely packed together. TEM observations of the same nanotube sample confirm that the constituent nanotubes have a hollow structure with a very narrow diameter distribution between 7 and 14 nm (Figure 3d,e) with mainly a double-walled nanotube structure (DWNT).[19] The SLVA-CNT array was used to prepare the CNT/polymer composite membrane by impregnating epoxy resin into gaps between the vertically aligned nanotubes, followed by removal of the polymer-coated nanotube film from the Si substrate and opening of the nanotube ends (Figure 1a).

Figure 4a shows a typical optical microscopic image for the SLVA-CNT/epoxy composite membrane thus prepared. As can be seen, a homogeneous large-area free-standing membrane was obtained. The corresponding AFM and SEM images for the shiny flat side of the membrane, given in Figure 4b and c, respectively, clearly show pores homogenously distributed over the whole membrane surface with an average pore size of about 10 nm, consistent with the TEM examination (Figure 3). The hole packing density of the nanotube membrane was estimated to be around $2.4 \times 10^{10}/\text{cm}^2$ based on the SEM and AFM images, which is consistent with the typical value ($\sim 10^{10}-10^{11}/\text{cm}^2$) of the CNT packing density for the as-synthesized vertically aligned carbon nanotubes.[25,26]

In order to ensure the as-prepared membrane is crack-free for the flow to pass through the nanotube hollow cores only, we filled a wine-red aqueous solution of 13 nm gold nanoparticles through the membrane. The permeated liquid showed no color, indicating

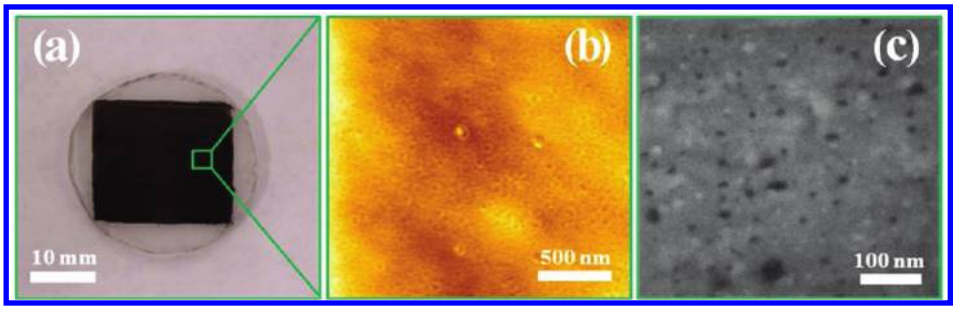

Figure 4. SLVA-CNT and epoxy membranes: (a) digital photograph of the 2 cm × 2 cm membrane; (b, c) AFM and SEM images of the SLVA-CNT and epoxy membrane surface under different magnifications.

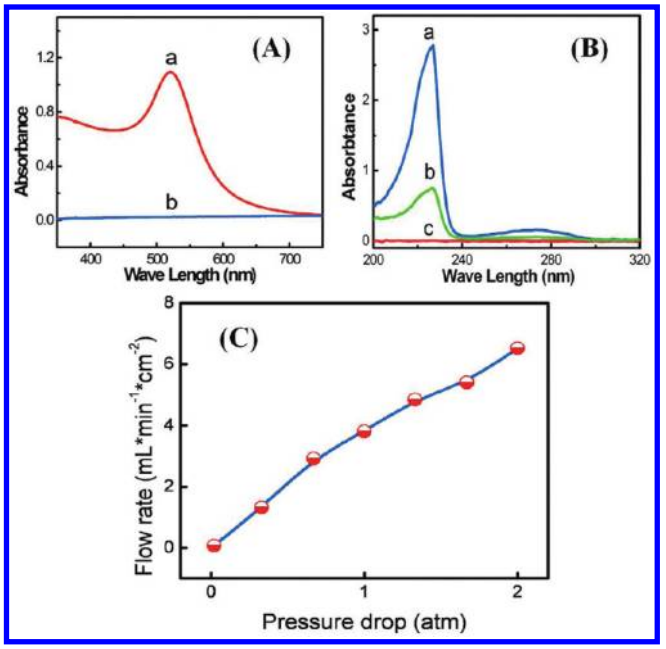

Figure 5. (A) UV−vis spectra of the nano gold solution (a) before and (b) after filtration. (B) UV−vis spectra of (a) dye molecules in water, (b) an aqueous solution after washing the broken SLVA-CNT and epoxy membrane, and (c) the permeated water solution after filtration through the pristine SLVA-CNT and epoxy membrane. (C) Dependence of flow rate on the pressure drop.

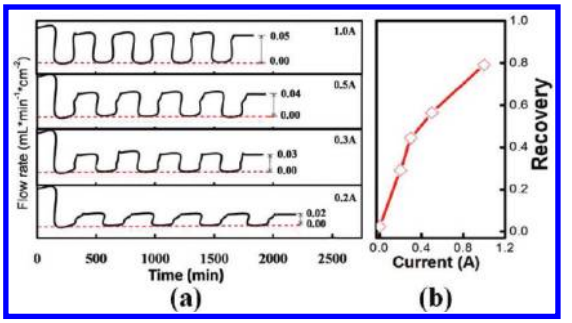

Figure 6. (a) Switching the flow through the SLVA-CNT and epoxy membrane on/off by applying different currents on the coils above/below the membrane in Figure 2. Red dotted lines represent the zero flow rate baselines. (b) Dependence of flow recovery percentage [defined as (final flow rate/initial flow rate), %] on applied current.

that the membrane is free from any microcracks, and hence the gold nanoparticles were completely blocked by the membrane. As expected, the pronounced surface plasmon resonance band around 530 nm, characteristic of the gold nanoparticles, seen for the starting nanogold solution in Figure 5A completely disappeared from the corresponding UV−vis spectrum of the permeated solution collected after filtration. Furthermore, we have also carried out UV−vis characterization for membranes based on the SLVA-CNT and epoxy mixed with dye molecules (i.e., 2-naphthalenesulfonic acid hydrate). As can be seen in Figure 5B, no observable dye molecules were detected in the permeated solution. However, a significant amount of dye molecules were observed in water used to wash a membrane that had been deliberately broken in pieces. These results clearly indicated that water did pass through the nanotube inner core but not the epoxy matrix.

The leak-free nanotube membrane (2 cm × 2 cm) was then investigated for water transport under ambient and 2 atm pressure. At ambient pressure, the volume flow rate for water to pass through the SLVA-CNT and epoxy membrane was found to be 0.27 mL/min, from which the corresponding volume flow rate through a single CNT and the associated flow speed were estimated to be 4.69×10^{-20} $m^3 \cdot s^{-1}$ and 5.97×10^{-4} m/s, respectively, given that the nanotube diameter is 10 nm and nanotube packing density is $2.4 \times 10^{10}/cm^2$ (vide supra). Upon increasing the pressure up to 2 atm (i.e., 1 atm pressure drop), the volume flow rate for water to pass through the same SLVA-CNT and epoxy membrane increased by a factor of 56 up to 15.20 mL/min (Figure 5C).[27] The corresponding volume flow rate through a single CNT and the flow speed became 2.64×10^{-18} $m^3 \cdot s^{-1}$ and 3.36×10^{-2} m/s, respectively. This value of the flow speed for a 4 mm thick SLVA-CNT (after cutting) membrane is significant, albeit it is slightly lower than 9.50×10^{-2} m/s reported for the shorter nanotube membrane of a comparable pore diameter.[7b]

To impart magnetically induced switching capability to the SLVA-CNT/epoxy composite membrane, we added 2 mL of an aqueous solution of iron nanoparticles (1 mg/mL) into 10 mL of water above the membrane (Figure 2) under ambient atmosphere. Subsequent application of a 0.4 A current on the coil below the membrane in Figure 2 generated a magnetic field, which attracted iron nanoparticles in the water solution above the membrane downward to completely block the CNT membrane within 2 min. As a result, only about 1 mL of water passed through the membrane for the following 150 min even in the absence of the magnetic field by turning off the current. However, the iron nanoparticle "stoppers" can be removed to open the membrane by simply applying a current with the same bias on the coil above the membrane (Figure 2). The membrane could be repeatedly switched on and off many times by applying

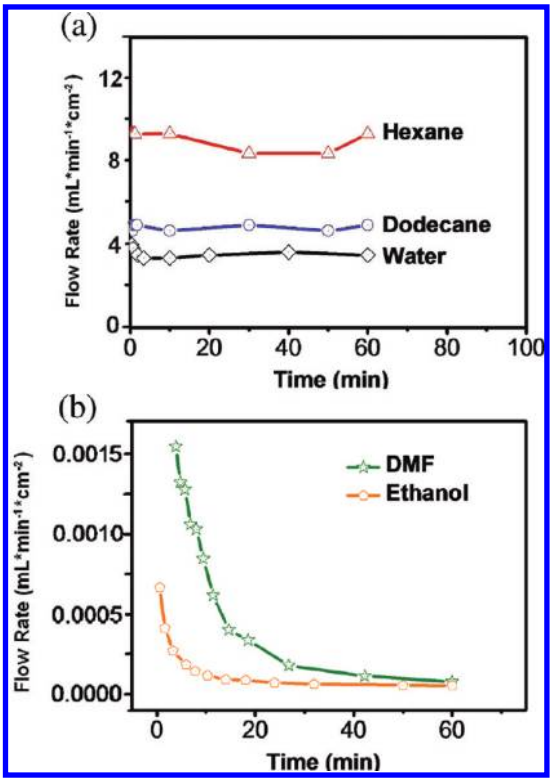

Figure 7. Flow rates for water, dodecane, hexane, DMF, and ethanol transport through SLVA-CNT/epoxy composite membrane of 0.72 cm^2 (cut from 2 cm × 2 cm sample to fit the stainless steel Millipore filter holder due to the size requirement) under a pressure of 2 atm.

alternative currents on the two coils. Figure 6a shows the switching characteristics for the SLVA-CNT/epoxy composite membrane under several different currents of 0.2, 0.3, 0.5, and 1.0 A, while Figure 6b shows the dependence of flow recovery percentage on the applied current. As can be seen in Figure 6, the observed on/off switching response to an applied current is reasonably fast with good repeatability and ~80% flow rate recovery at 1.0 A, though the diffusion rate of iron nanoparticles depends on the particle size and magnetic field strength. The membrane could be fully opened by removing all iron nanoparticles away from the membrane under a sufficiently strong magnetic field. However, the application of an excess amount of current may generate heat to overheat the system.

The above results prompted us to test the SLVA-CNT/epoxy composite membranes for mass transport with different solvents, including dodecane, hexane, *N*,*N* -dimethylformamide (DMF), and ethanol under 2 atm pressure. As can be seen in Figure 7a, hexane, dodecane, and water passed the membrane very quickly, but DMF and ethanol passed very slowly (Figure 7b). The initial relatively high flow rate for DMF (>40 min) and ethanol (>20 min) and the strong time dependence seen in Figure 7b were demonstrated to be caused by solvent absorption by the epoxy matrix. On the other hand, hexane, dodecane, and water might have shown negligible absorption into the epoxy matrix or the absorption, if any, has been obscured by the high flow rates seen in Figure 7a.

Table 1 shows the comparison of our permeability data with literature results[7b,8,16] for different solvents through CNT-based membranes. As can be seen, our superlong DWNT membrane shows relatively lower permeability but higher water/ethanol selectivity (Table 2) with respect to the MWNT membrane.[7b]

Assuming the systems investigated in the present study are Newtonian flows and follow the conventional Hagen−Poiseuille equation, $Q = (\pi d^4 \Delta p)/(128\eta L)$, we calculated the Q value from the volume flow rate (water, 2.51 mL/min; ethanol, 4.51×10^{-4} mL/min; DMF, 2.08×10^{-3} mL/min; dodecane, 3.53 mL/min; and hexane, 6.67 mL/min), membrane area of 0.72 cm^2, and CNT packing density of $2.4 \times 10^{10}/cm^2$. Here Q is the volumetric flow rate, Δp is the pressure drop (1.0 atm), L is the length of pipe (i.e., nanotube length; ~4 mm after cutting), η is the dynamic viscosity, and d is the pipe diameter (i.e., nanotube diameter; 10 nm). Table 3 lists the calculated results, along with the experimental data.

When the actual Q value from experimentally measured volume flow rates is compared with the calculated one, it seems that the nonpolar solvents (hexane and dodecane) showed 5−6 orders of magnitude faster than the conventional fluid flow. In contrast, the polar solvents (ethanol and DMF) showed only about 2 orders of magnitude faster than the conventional flow. Water differs from other solvents in that the "free" OH bond of water combines with the nanotube inner wall to form a depletion layer,[8] which reduces the number of hydrogen bonds in the depletion layer to reduce the friction and enhance the flow rate. Although ethanol also has the OH bond to form a depletion layer, each ethanol molecule has only one OH to combine with the nanotube inner wall to induce a relatively weak hydrogen-bond effect with respect to water.

The flow of different solvents through the nanotube channels was simulated via molecular dynamics (MD). Three types of solvents—water, ethanol (polar solvent), and hexane (nonpolar solvent)—were used to simulate the flow in the nanotube. The molecular configuration consists of a single-walled carbon nanotube, 5 nm in length and 2−4 nm in diameter (Figure 8). Periodic boundary conditions are applied in the nanotube-axis direction such that the tube represents an infinitely long tube configuration. The systems were relaxed at a constant pressure of 1 bar, a temperature of 300 K, and by use of the particle mesh Ewald method[28] for full electrostatics with a cutoff of 1 nm. After full relaxation, force was applied on each molecule to introduce pressure gradient for the flow. The behaviors of water, ethanol, and hexane are modeled by the potentials described in detail in refs 29−31, respectively. The predicted water flow rate in the nanotube is very close to that reported in ref 32. The simulation results show that the flow rates predicted from the MD simulations are much faster than those predicted from the Hagen−Poiseuille equation. Such flow rate enhancement is the result of the slip flow, which is governed by the liquid structure and collective molecular motion.[29−32]

The flow rate enhancement can be calculated by $\varepsilon = [1 + 8L_s/d]\text{-}(\mu_\infty/\mu)$, where d is the diameter, L_s is the slip length, and μ_∞ and μ are the bulk liquid viscosity and the diameter-specific fluid viscosity, respectively.[32] The parameters L_s and μ can be determined from the MD simulation; the detailed calculation procedure was described in ref 32. We have calculated the flow rate enhancement as 520, 45, and 730 for water, ethanol, and hexane, respectively, in a nanotube with d = 4 nm. Although the absolute values are not comparable to the experimental data listed in Table 3 due to technical difficulties in simulating the particular nanotubes (10 nm diameter) used in the membrane, the simulations do capture the difference in flow rate between these solvents. The low flow rate enhancement of ethanol may be attributed to the formation of molecular clusters due to O−H electrostatic attraction between ethanol molecules. It was found

Table 1. Permeability of Different Liquids through CNT Membranes[a]

	SLVA-DWNT membrane	multiwalled CNT[7b]	double-walled CNT[8]	polycarbonate membrane[8]
diameter (nm)	10	7	1.3−2.0	15
thickness (μm)	~4000	3−70	2−3	6
water permeability	3.9	$(5.7-26.3) \times 10^{2}$	$1.2-4.6 \times 10^{-1}$	$\sim 6.0 \times 10^{-3}$
ethanol permeability	6.3×10^{-4}	2.7×10^{2}		
hexane permeability	9.3	3.4×10^{2}		
decane permeability		4.0×10^{1}		
DMF permeability	2.9×10^{-3}			
dodecane permeability	4.9			
2-propanol permeability		6.7×10^{1}		

[a] Permeability is in the units $mL \cdot min^{-1} \cdot cm^{-2}$ at 1 atm.

Table 2. Comparison of Water/Ethanol Permeability Ratios from Three Different CNT Membranes

	SLVA-DWNT membrane	multiwalled CNT[7b]	multiwalled CNT[16]
dameter of carbon nanotube (nm)	10	7	43 ± 3
mmbrane thickness (μm)	~4000	3−70	78 ± 2
wter/ethanol permeability ratio	5.57×10^{3} (1 atm)	2.11−9.76 (1 atm)	1.25−1.47 (~3−8 kPa)

Table 3. Transport Characteristics for Water, Ethanol, DMF, Dodecane, and Hexane through SLVA-DWNT and Epoxy Membranes

	water	ethanol	DMF	dodecane	hexane
polarity index	9	5.2	6.4	0	0
viscosity (m Pa·s)	1.00	1.20	0.92	1.34	0.31
calcd Q ($m^3 \cdot s^{-1}$)	6.20×10^{-24}	5.18×10^{-24}	6.75×10^{-24}	4.64×10^{-24}	2.00×10^{-23}
actual Q ($m^3 \cdot s^{-1}$)	2.41×10^{-18}	4.82×10^{-22}	1.93×10^{-21}	3.40×10^{-18}	6.43×10^{-18}

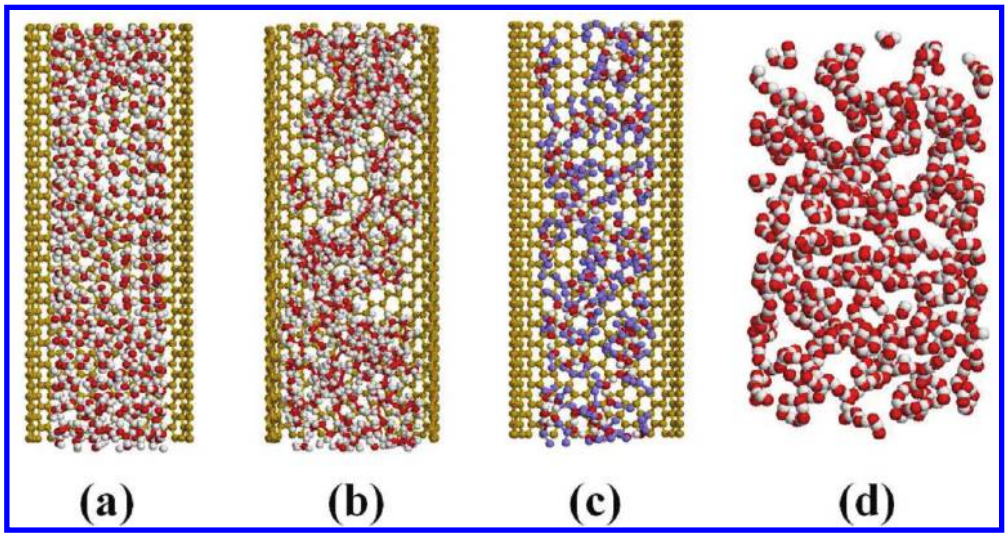

Figure 8. Molecular dynamics models for simulating the flow of (a) water, (b) hexane, (c) ethanol in a carbon nanotube of d = 2 nm, and (d) O−H bonding of ethanol in a carbon nanotube of d = 4 nm. In panel d carbon atoms are removed to better show the clustering structures of ethanol.

that ethanol molecules can form large molecular clusters in the nanotube (Figure 8d).

Since the molecular diameter of a single ethanol molecule is much larger than that of a water molecule, the clustering may significantly increase the viscosity. Our MD results show that the viscosity of ethanol is 183.2 mPa·s, 2−3 orders of magnitude higher than that of water (0.31 mPa·s) and hexane (0.09 mPa·s) within the nanotube. Although the results were obtained from

dx.doi.org/10.1021/la200995r |*Langmuir* 2011, 27, 8437–8443

a simulation of 4 nm nanotubes, we expect that viscosity will still be high in a 10 nm nanotube due to strong electrostatic interaction. Such high viscosity will significantly reduce the flow rate enhancement of the nanotube for ethanol.

Apart from the solvent effect discussed above, we have also investigated the CNT packing density effect by comparing the flow characteristics of SLVA-CNT and epoxy membranes with and without mechanical compression (Figure 1).[23] Water flow rates for the noncompressed (2 cm × 2 cm) and half-compressed (2 cm × 1 cm) SLVA-CNT/epoxy composite membranes were found to be 6.75×10^{-2} and 1.21×10^{-1} mL/cm^2·min, respectively. Therefore, the flow rate per unit area is directly proportional to the nanotube packing density in SLVA-CNT/epoxy composite membranes.

CONCLUSIONS

In summary, we have demonstrated a simple but effective method to prepare SLVA-CNT/epoxy composite membranes. Because of the low viscosity of epoxy polymer mixture for infiltration and the good properties of epoxy polymer, void-free CNT membranes were readily produced after solidification, which showed a significantly high flow rate for various liquids including water, hexane, and dodecane. These results were confirmed by molecular dynamics simulations. While mechanical compression was demonstrated to increase the flow rate, a magnetic coil was used to block and open the CNT membrane by applying currents to generate magnetic field to attract and remove iron nanoparticles to and from the membrane. The methodology developed in this study should have a significant implication for the development of various smart membranes in advanced intelligent systems.

AUTHOR INFORMATION

Corresponding Author
*E-mail liming.dai@case.edu.

ACKNOWLEDGMENT

We appreciate partial support from NSF (CMMI-1047655), DOE (DE-SC0003736), AFOSR (FA9550-10-1-0546), and AFOSR-MURI under Low Density Materials Program (Dr. Joycelyn Harrison, Program Manager). L.F. appreciates support from State Key Laboratory of Chemical Engineering (SKL-ChE-09D05), while L.Q. thanks support from the 111 Project B07012.

REFERENCES

(1) Harris, P. J. F. *Carbon Nanotubes and Related Structures: New Materials for the Twenty-First Century*; Cambridge University Press: New York, 1999.

(2) *Carbon Nanotechnology: Recent Developments in Chemistry, Physics, Materials Science and Device Applications*; Dai, L., Ed.; Elsevier: Amsterdam, 2006.

(3) Guldi, D. M.; Mamedov, A.; Crisp, T.; Kotov, N. A.; Hirsch, A.; Prato, M. *J. Phys. Chem. B* **2004**, *108*, 8770.

(4) Mamedov, A. A.; Kotov, N. A.; Prato, M.; Guldi, D. M.; Wicksted, J. P.; Hirsch, A. *Nat. Mater.* **2002**, *1*, 190.

(5) Giancane, G.; Ruland, A.; Sgobba, V.; Manno, D.; Serra, A.; Farinola, G. M.; Omar, O. H.; Guldi, D. M.; Valli, L. *Adv. Funct. Mater.* **2010**, *20*, 2481.

(6) Torsi, L.; Farinola, G. M.; Marinelli, F.; Tanses, M. C.; Omar, O. H.; Valli, L.; Babudri, F.; Palmisano, F.; Zambonin, P. G.; Naso, F. *Nat. Mater.* **2008**, *7*, 412.

(7) (a) Hinds, B. J.; Chopra, N.; Rantell, T.; Andrews, R.; Gavalas, V.; Bachas, L. G. *Science* **2004**, *303*, 62. (b) Majumder, M.; Chopra, N.; Andrews, R.; Hinds, B. J. *Nature* **2005**, *438*, 44. (c) Nednoor, P.; Gavalas, V. G.; Chopra, N.; Hinds, B. J.; Bachas, L. G. *J. Mater. Chem.* **2007**, *17*, 1755 and references cited therein.

(8) Holt, J. K.; Park, H. G.; Wang, Y.; Stadermann, M.; Artyukhin, A. B.; Grigoropoulos, C. P.; Noy, A.; Bakajin, O. *Science* **2006**, *312*, 1034.

(9) Won, C. Y.; Aluru, N. R. *Chem. Commun.* **2007**, *129*, 2748.

(10) Goel, G.; Krekelberg, W. P.; Errington, J. R.; Truskett, T. M. *Phys. Rev. Lett.* **2008**, *100*, No. 106001.

(11) Mittal, J.; Errington, J. R.; Truskett, T. M. *J. Phys. Chem. B* **2007**, *111*, 10054.

(12) (a) Skoulidas, A. L.; Ackerman, D. M.; Johnson, J. K.; Sholl, D. S. *Phys. Rev. Lett.* **2002**, *89*, 185901. (b) Hummer, G.; Rasaiah, J. C.; Noworyta, J. P. *Nature* **2001**, *414*, 188.

(13) Hinds, B. In *Carbon Nanotechnology: Recent Developments in Chemistry, Physics, Materials Science and Device Applications*; Dai, L., Ed.; Elsevier: Amsterdam, 2006.

(14) Cooper, S. M.; Cruden, B. A.; Meyyappan, M.; Raju, R.; Roy, S. *Nano Lett.* **2004**, *4*, 377.

(15) Chopra, N.; Majumder, M.; Hinds, B. J. *Adv. Funct. Mater.* **2005**, *15*, 858.

(16) Whitby, M.; Cagnon, L.; Thanou, M.; Quirke, N. *Nano Lett.* **2008**, *8*, 2632.

(17) Hata, K.; Futaba, D. N.; Mizuno, K.; Namai, T.; Yumura, M.; Iijima, S. *Science* **2002**, *306*, 1362.

(18) Liu, J.; Dai, L.; Baur, J. W. *J. Appl. Phys.* **2007**, *101*, No. 064312.

(19) Chakrabarti, S.; Gong, K.; Dai, L. *J. Phys. Chem. C* **2008**, *112*, 8136.

(20) Gong, K.; Chakrabarti, S.; Dai, L. *Angew. Chem., Int. Ed.* **2008**, *47*, 5446.

(21) Lee, C. Y.; Choi, W.; Han, J. H.; Strano, M. S. *Science* **2010**, *329*, 1320.

(22) Lee, K. M.; Li, L. C.; Dai, L. M. *J. Am. Chem. Soc.* **2005**, *127*, 4122.

(23) Wardle, B. L.; Saito, D. S.; García, E. J.; Hart, A. J.; Villoria, R. G.; de, Verploegen, E. A. *Adv. Mater.* **2008**, *20*, 2707.

(24) Chang, D. W.; Dai, L. *Nanotechnology* **2007**, *18*, No. 365605 and references cited therein.

(25) Qu, L.; Dai, L. *Adv. Mater.* **2007**, *19*, 3844.

(26) Qu, L.; Dai, L.; Stone, M.; Xia, Z.; Wang, Z. L. *Science* **2008**, *322*, 238.

(27) By assuming that the water flow through CNT membrane is a Newtonian flow, we calculated the pressure-induced flow rate enhancement by the conventional Hagen−Poiseuille equation: $Q = (\pi d^4 \Delta p)/(128\eta L)$, where Q is the volumetric flow rate, Δp is the pressure drop, L is the length of pipe, η is the dynamic viscosity, and d is the pipe diameter. Since L, η, and d are constant in this particular case, the Q value depends only on the pressure drop (Δp). In the case where no additional pressure is applied, the pressure drop comes from the gravity of water column. So, the pressure drop here is 20-cm water held in a burette. Upon increasing the pressure up to two atmosphere pressures, the pressure drop is around 1 atm; equivalent to 10.3-m height water. Therefore, Q (additional 1 atm)/Q (no additional pressure) = Δp (additional 1 atm)/Δp (no additional pressure) = 10.3 m water height / 0.2 m water height = 51.5 times, showing good consistency with the experiment result (around 56 times).

(28) Darden, T. A.; York, D. M.; Pedersen, L. G. *J. Chem. Phys.* **1993**, *98*, 10089.

(29) Gong, X.; Li, J.; Lu, H.; Wan, R.; Li, J.; Hu, J.; Fang, H. *Nat. Nanotechnol.* **2007**, *2*, 709.

(30) Connolly, M. J.; Roth, M. W.; Gray, P. A.; Wexler, C. *Langmuir* **2008**, *24*, 3228.

(31) Shao, Q.; Huang, L.; Zhou, J.; Lu, L.; Zhang, L.; Lu, X.; Jiang, S.; Gubbins, K. E.; Zhu, Y.; Shen, W. *J. Phys. Chem. C* **2007**, *111*, 15677.

(32) Thomas, J. A.; McGaughey, A. J. H.; Kuter-Arnebeck, O. *Int. J. Therm. Sci.* **2010**, *49*, 281.